Site-specific atomic substitution in a giant magnetocaloric Fe₂P-type system

Sagar Ghorai [ORCID],[1,*] Johan Cedervall [ORCID],[2] Rebecca Clulow,[3] Shuo Huang,[4,5] Tore Ericsson,[3] Lennart Häggström,[3]
Vitalii Shtender [ORCID],[3] Erna K. Delczeg-Czirjak [ORCID],[6] Levente Vitos,[5] Olle Eriksson,[6] Martin Sahlberg,[3] and Peter Svedlindh[1]

[1]*Department of Materials Science and Engineering, Uppsala University, Box 35, SE-751 03 Uppsala, Sweden*
[2]*Department of Materials and Environmental Chemistry, Stockholm University, SE-10691 Stockholm, Sweden*
[3]*Department of Chemistry – Ångström Laboratory, Uppsala University, Box 538, Uppsala 75121, Sweden*
[4]*Faculty of Materials Science and Chemistry, China University of Geosciences, Wuhan 430074, China*
[5]*Department of Materials Science and Engineering, Royal Institute of Technology, Stockholm SE-100 44, Sweden*
[6]*Department of Physics and Astronomy, Uppsala University, Box 516, SE-751 20 Uppsala, Sweden*

Giant magnetocaloric (GMC) materials constitute a requirement for near-room-temperature magnetic refrigeration. (Fe,Mn)₂(P,Si) is a GMC compound with strong magnetoelastic coupling. The main hindrance towards application of this material is a comparably large temperature hysteresis, which can be reduced by metal site substitution with a nonmagnetic element. However, the (Fe,Mn)₂(P,Si) compound has two equally populated metal sites, the tetrahedrally coordinated $3f$ and the pyramidally coordinated $3g$ sites. The magnetic and magnetocaloric properties of such compounds are highly sensitive to the site-specific occupancy of the magnetic atoms. Here we have attempted to study separately the effect of $3f$ and $3g$ site substitution with equal amounts of vanadium. Using formation energy calculations, the site preference of vanadium and its influence on the magnetic phase formation are described. A large difference in the isothermal entropy change (as high as 44%) with substitution in the $3f$ and $3g$ sites is observed. The role of the lattice parameter change with temperature and the strength of the magnetoelastic coupling on the magnetic properties are highlighted.

I. INTRODUCTION

Replacement of conventional vapor compression refrigeration with a 20–30 % more efficient solid-state magnetic refrigeration technique based on the magnetocaloric effect has the additional advantage of reducing emission of greenhouse gases [1]. To build a magnetic refrigerator that can work near room temperature, materials with a giant magnetocaloric (GMC) effect and a magnetic phase transition temperature near room temperature are required. In this regard, several GMC materials with first-order magnetic phase transitions have been proposed [2]. Despite high values of the isothermal entropy change and adiabatic temperature change, these first-order materials may not be suitable for magnetic refrigeration owing to a large temperature hysteresis (ΔT_{hys}). ΔT_{hys} represents the irreversible nature of the temperature-dependent magnetic phase change, which is a drawback for magnetic refrigeration [3]. While several ways of reducing ΔT_{hys} have been attempted [3,4], the basic origin of ΔT_{hys} is still unclear. Here in this work we provide an explanation for the origin of ΔT_{hys} in the context of magnetoelastic coupling of (Fe,Mn)₂(P,Si)-type materials. (Fe,Mn)₂(P,Si)-type materials constitute a class of GMC materials consisting of

earth-abundant, environment-friendly, and nontoxic elements. These compounds crystallize in a hexagonal Fe₂P-type structure (space group $P\bar{6}2m$). In the hexagonal structure the metallic atoms occupy the $3f$ and $3g$ sites while the nonmetallic atoms occupy the $1b$ and $2c$ sites [5,6]. From electronic structure calculations [7], the observed magnetoelastic coupling for this series of compounds has been explained by a drastic fall of the magnetic moment of Fe ($1.54\mu_B$/atom to $\sim 0.003\mu_B$/atom) while it transforms from the ferromagnetic (FM) to the paramagnetic (PM) state. This moment change occurs due to the fact that the nonbonded or metallic Fe below the Curie temperature (T_C) hybridizes with Si/P above T_C. The hybridization around T_C causes a drastic change of the hexagonal lattice parameters and a strong magnetoelastic coupling results [7]. For GMC materials, a high magnetization is beneficial, which is mainly provided by the Mn atoms. It can be stated as that the Fe atoms maintain the first-order phase transition, while Mn atoms maintain the overall magnetization of (Fe,Mn)₂(P,Si)-type materials. To understand the effect of these two phenomena, Fe and Mn atoms are individually attempted to be replaced with nonmagnetic V in this work. Recently Lai *et al.* [8,9] have discussed the reduction of ΔT_{hys} with V substitution in the metallic sites. However, the occupation of V in the metallic sites (i.e., $3f$ or $3g$ sites) is still unclear. Interestingly, the magnetic atoms exhibit different magnetic moments depending upon their site occupancy [10], yielding completely different magnetic and magnetocaloric properties [e.g., T_C, saturation magnetization (M_S), isothermal entropy change ($-\Delta S_M$), ΔT_{hys}, etc.]. Here, in this work we have attempted to substitute the $3g$ and $3f$ sites of the parent compound FeMnP₀.₅Si₀.₅ individually with 5 at% of V. Both

site substitutions exhibit a small difference in the T_C values, while there is a large difference ($\sim$44% at $\mu_0 H = 2$T) in the value of $-\Delta S_M$. This difference is explained by the strength of the magnetoelastic coupling and the preferred occupancy of V.

II. EXPERIMENTAL DETAILS AND CALCULATION METHOD

All compounds were synthesized by the drop synthesis method [11]. Further, the vacuum-sealed samples (pressed pellets) were sintered at 1373 K for 1 h, followed by annealing at 1073 K for 65 h before being quenched in ice water. X-ray powder diffraction (XRPD) data were collected at different temperatures ranging from 265 K–422 K using a Bruker D8 Advance diffractometer with Cu-K$_{\alpha 1}$ radiation, with an angle step size of 0.02°. Variable temperature XRD data were analyzed using Pawley refinements within the TOPAS6 software program [12]. Mössbauer measurements were carried out on a constant acceleration spectrometer with a ^{57}CoRh source. The samples were enclosed in sealed kapton pockets yielding a sample concentration of $\approx$10 mg/cm^2. Calibration spectra were recorded at 295 K using natural Fe metal foil as a reference absorber. The spectra were recorded at 410 K and fitted using the least-square Mössbauer fitting program RECOIL to obtain the values of the center shift CS, the magnitude of the electric quadrupole splitting $|QS|$, the full-width at half-maxima W of the Lorentzian absorption lines and the spectral intensities I. Magnetic properties were measured in the temperature range from 5 K–400 K using Quantum Design MPMS-XL and PPMS systems with a maximum magnetic field of 5 T. EDX (energy dispersive x-ray) measurements were performed on a Zeiss Leo 1550 field emission SEM (scanning electron microscope) equipped with Aztec energy dispersive x-ray detector. Data were collected on at least ten spots of each sample using an accelerating voltage of 20 kV by and EDX mapping was carried out on regions of approximately 300 μm × 300 μm.

The total energy calculations were carried out by the exact muffin-tin orbitals (EMTO) method in combination with the coherent potential approximation (CPA) [13]. The one-electron Kohn-Sham equation was solved within the softcore and scalar-relativistic approximations. The s, p, d, and f orbitals were included in the muffin-tin basis set. The Green's function was calculated by using 16 complex energy points on a semicircular contour including the valence states. The exchange-correlation interactions were treated within the generalized gradient approximation in the form of Perdew-Burke-Ernzerhof (PBE) [14]. Further details about the adopted method can be found in previous work [13]. For the further discussion the parent compound, FeMnP$_{0.5}$Si$_{0.5}$ and the two V-substituted compounds FeMn$_{0.95}$V$_{0.05}$P$_{0.5}$Si$_{0.5}$ (3g site substituted) and Fe$_{0.95}$V$_{0.05}$MnP$_{0.5}$Si$_{0.5}$ (3f site substituted) are abbreviated as P, V3g, and V3f, respectively.

III. RESULTS AND DISCUSSION

A. Magnetoelastic coupling and magnetocaloric effect

The magnetocaloric effect is often characterized with the isothermal entropy change ($-\Delta S_M$). The total entropy of a system is the sum of magnetic, lattice and electronic entropy contributions of the system. For a first-order magnetic phase transition (i.e., a system with a discontinuity in the first-order derivative of the Gibbs free energy) the magnetic phase transition is often associated with a lattice or electronic phase transition. Moreover, if this is the case, a high value of $-\Delta S_M$ is expected.

The (Fe,Mn)$_2$(P,Si) system shows a first-order magnetoelastic phase transition, where a sharp change of the hexagonal lattice parameter ratio c/a (keeping the lattice volume almost constant) occurs in the vicinity of the magnetic phase transition. Hence, the total entropy change of the system includes both magnetic and lattice entropy contributions. In our studied compounds a temperature-dependent change of the c/a ratio from a high value ($\sim$0.57) to a relatively lower value ($\sim$0.53) has been observed when the system transforms from the PM to the FM state. At high temperature ($>T_C + 30$ K) the system corresponds fully to a Fe$_2$P-type phase with a high c/a ratio, while at a sufficiently low temperature ($< T_C - 100$ K) the system corresponds fully to a Fe$_2$P-type phase with a low c/a ratio. Therefore, near T_C, contributions (phase wt%) from both Fe$_2$P-type phases with high and low c/a ratios are present. From the collected XRPD patterns, the temperature-dependent variation of two Fe$_2$P-type phases are shown in Fig. 1(a). The crossing point of the two Fe$_2$P phases represent the c/a transition temperature, i.e., the structural phase transition temperature [T_{st}, cf. Fig. 1(a)]. The strength of the magnetoelastic coupling depends upon two factors; first the degree of structural change, in this case the variation of the c/a ratio ($\Delta(c/a)$, for calculation see Supplemental Material [15]), which is shown in the inset of Fig. 1(a), and second the difference between the structural and magnetic phase transition temperatures. From the relative difference between T_{st} and T_C [cf. Fig. 1(a)] and the change of absolute value of c/a [$\Delta(c/a)$], it is clear that the magnetoelastic coupling strength is highest for the parent compound (P) followed in descending order by the V3g and V3f compounds. As discussed before, the strength of magnetoelastic coupling has a direct influence on the value of $-\Delta S_M$. The value of $-\Delta S_M$ has been calculated using the Maxwell relation [16], $\Delta S_M(T, H_f) = \mu_0 \int_0^{H_f} (\frac{\delta M(H,T)}{\delta T})_H \, dH$, for a magnetic field change of H_f. The magnetic isotherms have been recorded during cooling of the material with a cyclic measurement protocol [17], where the sample is subsequently heated to its PM state before stabilizing at the temperature of the measurement. The calculated values of $-\Delta S_M$ are presented in Fig. 1(b). The values of $-\Delta S_M$ follows the same trend as that of the magnetoelastic coupling strength, i.e., the highest value for the parent compound followed by lower values for the V3g and V3f compounds. This is a manifestation of the proportionality between the magnetoelastic coupling strength and $-\Delta S_M$.

To estimate the temperature range of the materials to be useful as a magnetic refrigerant, the relative cooling power (RCP) is often used [25]. The RCP value can be calculated from the temperature-dependent $-\Delta S_M$ curve as $RCP = -\Delta S_M^{\max} \times \Delta T_{\text{FWHM}}$, where $-\Delta S_M^{\max}$ is the maximum of the isothermal entropy change and ΔT_{FWHM} is the full-width at half-maximum of the temperature-dependent $-\Delta S_M$ curve. Here the RCP and $-\Delta S_M$ values of the studied compounds along with the corresponding
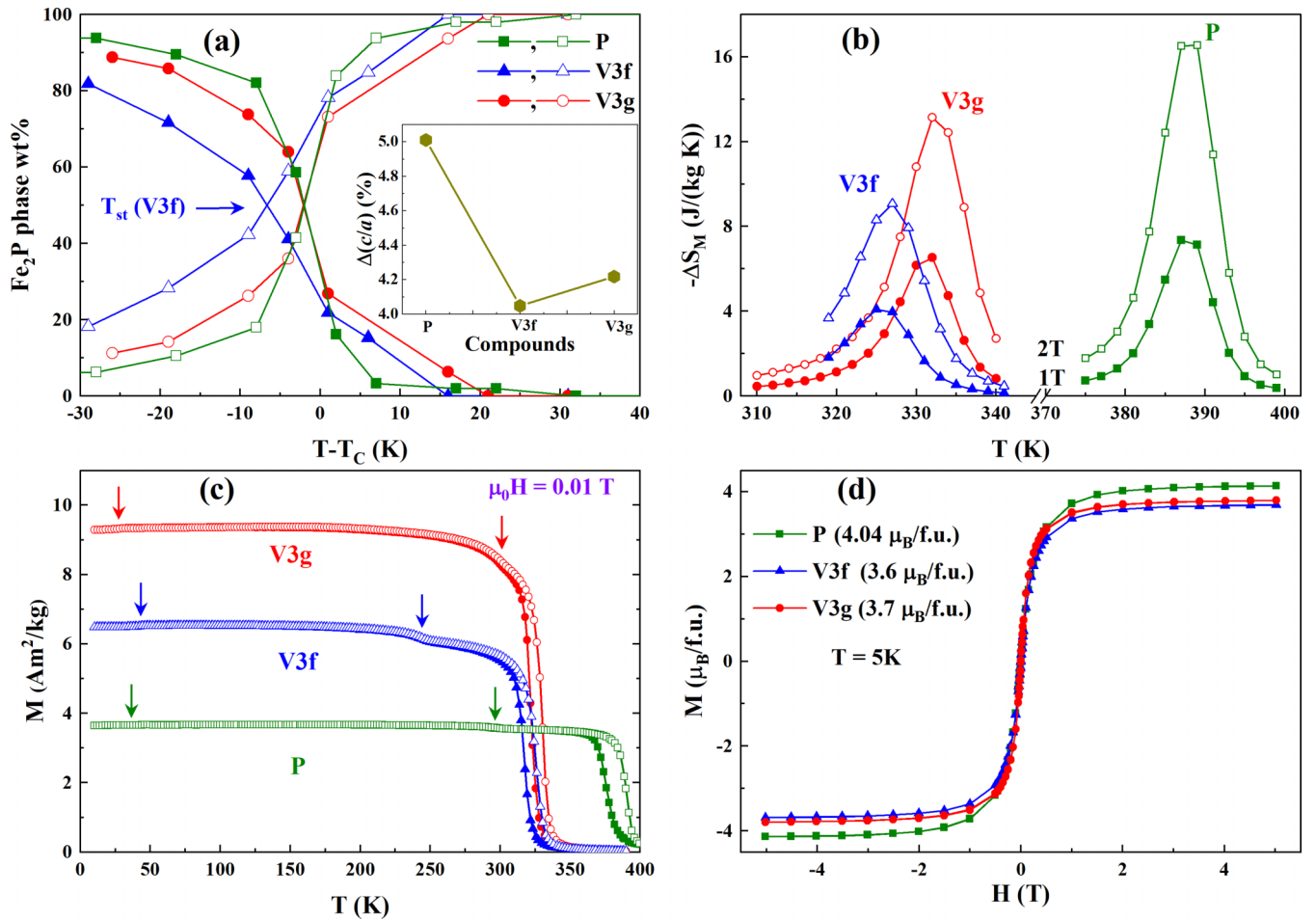
FIG. 1. (a) Temperature-dependent variation of the Fe_2P phases with low ($\sim$0.53) and high ($\sim$0.57) c/a ratio represented by solid and hollow symbols, respectively. The crossing points of the two Fe_2P phases represent the structural transition temperatures T_{st} of the studied compounds (for the V3f compound, T_{st} is indicated by the blue arrow). (b) Temperature-dependent variation of the isothermal entropy change, hollow (solid) symbols represent data at a magnetic field change of 2 T (1 T). (c) Temperature-dependent variation of the magnetization at $\mu_0 H = 0.01$ T. The solid and hollow symbols represent data collected during field cooling and subsequently during field-cooled warming, respectively. The arrows indicate phase transition temperatures of the (Fe,Mn)$_3$Si-type impurity phase. (d) Isothermal magnetization at 5 K for the different compounds.

data for some well-known GMC materials are listed in Table I.

B. Curie temperature and hysteresis

For a material to be useful in room-temperature magnetic refrigeration, the first requirement is to have a magnetic phase transition temperature near room temperature. Figure 1(c) shows magnetization versus temperature curves for the different compounds measured during field cooling (FC) and subsequently during field-cooled warming (FCW). The parent compound (FeMnP$_{0.5}$Si$_{0.5}$) has a T_C value of around 380 K. With 5 at% V substitution in either of the metallic sites (it will later be shown that V substituting in the 3g site is energetically more favorable), T_C decreases and comes closer ($\sim$320 K) to room temperature [cf. Fig. 1(c)], making this substitution process useful for magnetic refrigeration. Apart from the PM to FM phase transition, two additional kinks (marked with arrows) are observed in the temperature-dependent magnetization curves (cf. Fig. 1(c) and Supplemental Material [15]),

owing to the presence of a (Fe,Mn)$_3$Si-type impurity phase. The details of this impurity phase formation will be discussed later. The value of T_C corresponds to the amount of thermal energy required to transform a material from its magnetically ordered state to a magnetically disordered state, therefore the value of T_C is directly related to the strength of the exchange interaction between the spins of the magnetic atoms. Moreover, the exchange interaction between spins is highly sensitive to the interspin distance. From neutron diffraction [5,6] and Mössbauer spectroscopy [26] results, it has been observed that in the (Fe,Mn)$_2$(P,Si) system, Fe, Mn, and P/Si occupy the 3f, 3g, and 1b/2c sites of the hexagonal lattice, respectively. Among them, the magnetic atoms Fe and Mn are separated along the c axis and distributed in the ab plane. Therefore, changes of the lattice parameters c and a will influence the distance between the Fe and Mn atoms. From temperature-dependent XRPD results, the variation of the lattice parameter c with temperature for every compound is depicted in Fig. 2(a). It should be kept in mind that near T_C all compounds have two Fe_2P-type phases with different

TABLE I. Magnetocaloric properties of the studied compounds (*) compared with data reported for other GMC materials near room temperature. The values of T_C for the studied compounds are taken from the FC magnetization versus temperature curves.

Sample	T_C (K)	$\mu_0 H$ (T)	$-\Delta S_M$ (J/kgK)	RCP (J/kg)	Ref.
FeMnP$_{0.5}$Si$_{0.5}$(P)	376	2	16.5	147	*
Fe$_{0.95}$V$_{0.05}$MnP$_{0.5}$Si$_{0.5}$(V3f)	318	2	9.1	103	*
FeMn$_{0.95}$V$_{0.05}$P$_{0.5}$Si$_{0.5}$(V3g)	322	2	13.1	130	*
Gd	295	2	6.1	240	[18]
La(Fe$_{0.98}$Mn$_{0.02}$)$_{11.7}$Si$_{1.3}$H	312	2	13	–	[19]
La$_{0.67}$Ca$_{0.33}$MnO$_3$	260	1.5	4.3	47	[20]
La$_{0.5}$Pr$_{0.2}$Ca$_{0.1}$Sr$_{0.2}$MnO$_3$	296	2	1.8	147	[21]
Fe$_{80}$Pt$_{20}$	290	2	∼10	–	[22]
Mn$_{1.2}$Fe$_{0.8}$P$_{0.75}$Ge$_{0.25}$	288	2	20	–	[23]
MnFeP$_{0.52}$Si$_{0.48}$	268	2	10	–	[24]

c/a ratios. Among them, the low c/a ratio is dominant below T_C and vice versa. Therefore, in the following discussion, only the dominant Fe$_2$P phase is considered. From Figs. 2(a)
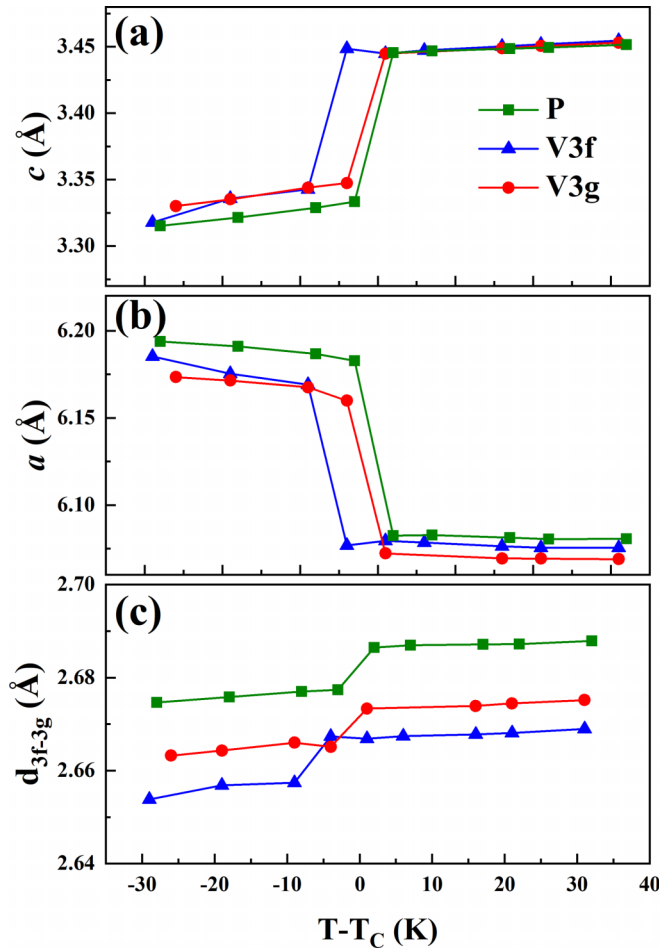

FIG. 2. Temperature-dependent variation of the hexagonal lattice parameters; (a) c, (b) a, and (c) atomic distance between the 3f and 3g sites. The error in the lattice parameter data is in the order of 10^{-4} Å.

and 2(b), it is observed that close to magnetic transition temperature there is a large decrease (for the dominant Fe$_2$P phase) of the lattice parameter c and a large increase in the lattice parameter a. However, it is not straightforward to find a direct relationship between the lattice parameters and the distance between magnetic atoms (Fe and Mn) owing to the presence of two Fe$_2$P phases along with a (Fe,Mn)$_3$Si-type impurity phase. In an attempt to find a relationship, one can consider the previously proposed distance d_{3f-3g} between the 3f and 3g sites for a pure Fe$_2$P system [11],

$$d_{3f-3g} = \sqrt{[(y-x) \times a]^2 + [0.5 \times c]^2}, \quad (1)$$

where the positions of 3f and 3g site atoms are $(x, 0, 0)$ and $(y, 0, 0.5)$, respectively. From the Rietveld refinement of the room-temperature XRPD patterns of the studied compounds, the values of x and y have been determined as 0.2577(1) and 0.5966(1) for the parent compound P; 0.2581(1) and 0.5930(1) for the compound $V3f$; and 0.2561(1) and 0.5928(1) for the compound $V3g$. Assuming a negligible temperature dependence of the atomic coordinates the calculated values of d_{3f-3g} are shown in Fig. 2(c). A decrease of d_{3f-3g} at the PM to FM phase transition is observed for all three compounds. This trend of a decreasing 3f-3g atomic distance at the PM to FM phase transition is in good agreement with that observed for the pure Fe$_2$P compound [27] (see Supplemental Material [15]). From Fig. 2(c), it is observed that the value of d_{3f-3g} is highest for the compound P, followed by the $V3g$ and $V3f$ compounds in descending order.

The Bethe-Slater (BS) curve provides a relationship between the nearest-neighbor distance between atoms normalized with the radius of the 3d shell and the direct exchange interaction (J) [28]. The BS curve is known to successfully describe the transition from antiferromagnetic (AFM) to ferromagnetic (FM) spin order when traversing the elements of the 3d transition series. A reasonable assumption for the compounds studied here is that their normalized nearest-neighbor distances will fall in between those of manganese and iron and that a smaller value of d_{3f-3g} will correspond to a smaller value of J. Thus, according to the BS curve, given that there is a proportionality between T_C and J, the decrease of T_C for the P-$V3g$-$V3f$ compounds (see Table I) can be explained by a decrease of d_{3f-3g}.

Fe and Si both occupy the same basal plane, thus an increase of the a parameter during the PM to FM phase transition [cf. Fig. 2(b)] favors localization of the 3d electrons and less bonding with Si atoms. From DFT calculation results [7,29] of (Fe,Mn)$_2$(P,Si) system, it has been observed that the density of states (DOS) of Mn 3d electrons remains identical in the FM and PM states while the DOS of the Fe 3d electrons is significantly different comparing the FM and PM states. In fact, the change of the local magnetic moment of Fe has been identified as the reason for observing the magnetoelastic coupling in the (Fe,Mn)$_2$(P,Si) system [30]. Moreover, the increment of the a lattice parameter, across the PM to FM transition represents a strong magnetoelastic coupling. The variation of the c parameter, and the a parameter (Δc, and Δa, respectively, see Table II) are the largest for the parent compound, followed by the V3g and V3f compounds. The reason for the strong first-order character of the magnetic

TABLE II. Magnetic and magnetoelastic properties. The value of T_C is taken from the FC magnetization versus temperature curve, while ΔT_{hys} is defined as the difference in transition temperature between the FCW and FC magnetization curves.

Sample	T_C (K)	$\|\Delta c\|$ (%)	$\|\Delta a\|$ (%)	ΔT_{hys} (K)	M_S ($\mu_B/f.u.$)
P	376	3.30	1.64	22	4.04
V3f	318	2.64	1.34	8.5	3.6
V3g	322	2.80	1.44	8.5	3.7

phase transition is that the magnetic and structural phase transitions occur in a narrow temperature interval, i.e., the phase transitions are coupled. The two Fe_2P-type phases, characterized by different a and c parameters are separated by an energy barrier, which is responsible for the temperature hysteresis (ΔT_{hys}) of these materials [31]. Table II shows the variation of the lattice parameters ($\Delta a/a$ and $\Delta c/c$) across the magnetic transition indicating that the parent compound has the strongest magnetoelastic coupling or largest energy barrier, resulting in a relatively larger value of ΔT_{hys}. On the contrary, the relatively lower values of $\Delta a/a$ and $\Delta c/c$ for the V3f and V3g compounds yield reduced values of ΔT_{hys}. For the reversibility of a magnetic heat pump, a minimal value of ΔT_{hys} is required [3], indicating that V substitution constitutes a useful process for magnetic refrigeration applications.

C. Magnetization anomaly and Mössbauer spectra

Theoretical calculations of the site-specific magnetic moment of the parent compound (FeMnP$_{0.5}$Si$_{0.5}$) show that the magnetic moments of Mn in the 3g site and Fe in the 3f site are 2.81 μ_B/atom and 1.68 μ_B/atom, respectively [10]. Therefore, substitution with nonmagnetic V is expected to reduce the overall magnetization more for 3g-site substitution compared to 3f-site substitution. However, an inverse behavior is observed from the values of the saturation magnetization [cf. Fig. 1(d) and Table II]. A possible reason for this anomaly could be a partly random occupancy of Fe and Mn atoms, i.e., if some amount of Fe (Mn) is distributed in the 3g (3f) site. To investigate this possibility, we have collected Mössbauer spectra for the compounds in their paramagnetic states.

In Fig. 3, the Mössbauer spectra of the three studied compounds are shown. For the parent compound, FeMnP$_{0.5}$Si$_{0.5}$, the broadenings emanate from the different surroundings of Fe at the metal 3f site. There are four near-neighbor elements P and Si, two occupying the 1b and two the 2c sites. It has been shown that Si prefers the 2c site almost exclusively [32]. For the present compound, two P atoms will occupy the two nearest 1b sites, and assuming random occupation on the 2c sites we would expect three different near-neighbor surroundings; P$_2$Si$_2$ (i.e., one Fe atom is surrounded by two P and two Si atoms), P$_3$Si$_1$ and P$_4$ with probabilities of 0.5625, 0.375, and 0.0625, respectively. These components are shown in Fig. 3 with red, green, and blue subpatterns, respectively. Accordingly, the spectra at 410 K, irrespective of V content were fitted with three doublets. The fitting results for the average hyperfine values are presented in Table III. The CS values for the V-substituted samples have decreased as compared
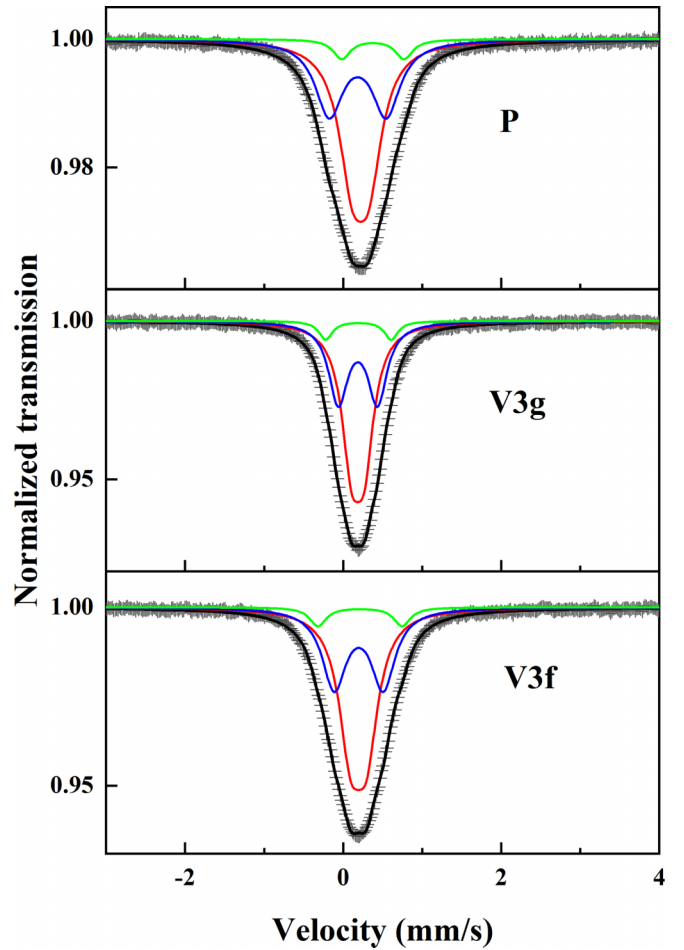

FIG. 3. Mössbauer spectra of the studied compounds at 410K. The red, blue, and green subpatterns correspond to the nearest-neighbor surroundings (P$_2$Si$_2$), (P$_3$Si$_1$), and (P$_4$) of Fe at the 3f site, respectively.

to the value for the parent sample. It should be noted that a decrease in CS corresponds to an increase in electron density at the Fe nuclei [33,34]. This increase in Fe electron density can be related to the V substitution in the 3f and 3g sites. Moreover, the increase in electron density at the Fe nuclei favors Fe bonding with nonmetallic atoms and prevents the desired moment fluctuation at the PM to FM phase transition. A larger moment fluctuation will result in a larger change of magnetic entropy and hence a larger value of $-\Delta S_M$. The same trend for the values of CS and $-\Delta S_M$ confirms the theoretical prediction [30] of the moment fluctuation of Fe in the 3f site.

The broad single line centered around 0.2 mm/s matches well with results from a previous study [10] and evidences that

TABLE III. Results from fitting of Mössbauer spectra.

Sample	CS (± 0.005)	$\|QS\|$ (± 0.005)	W (± 0.005)
P	0.220	0.210	0.406
V3g	0.193	0.336	0.558
V3f	0.185	0.279	0.443

TABLE IV. Chemical composition of the studied compounds from EDX analysis.

Element (at%)	P	V3f	V3g
Fe (expected)	33.33	31.67	33.33
Fe (observed)	33(3)	31(2)	31(2)
Mn (expected)	33.33	33.33	31.67
Mn (observed)	35(3)	34(2)	31(1)
V (expected)	0	1.67	1.67
V (observed)	0	1.9(6)	1.7(2)
P (expected)	16.67	16.67	16.67
P (observed)	16(3)	16(3)	18(2)
Si (expected)	16.67	16.67	16.67
Si (observed)	15(2)	17(2)	19(2)

Fe atoms occupy the 3f site. Also, the absence of any high-velocity resonance line or shoulder diminishes the possibility of Fe 3g site occupation.

D. Chemical composition and magnetic phases

The chemical compositions of the compounds as obtained from analysis of the EDX results are listed in Table IV.

From Table IV it is clear that all the compounds have the expected chemical composition within the margin of error. However, during analysis of the EDX results some Si-rich portions have been identified. As indicated in the Supplemental Material [15], from the elemental mapping of P it is clear that the above-mentioned Si-rich portions exhibit P deficiency. Typically, these Si-rich or P-deficient portions [cf. Figs. 4(a)–4(c)] correspond to a (Fe,Mn)$_3$Si phase. From the room-temperature XRPD analysis a small amount ($\sim$5 at%) of (Fe,Mn)$_3$Si phase has been identified for the three compounds. Formation of this secondary phase indicates a possible loss of P during synthesis. However, the analysis of the EDX results exhibits a large error bar (as high as 3 at% for the Fe and Mn content) and the XRPD refinement with multiple phases is not very sensitive to Fe/Mn intermixing. Fortunately, the magnetic properties of the secondary phase can be used to predict the Fe to Mn ratio. The (Fe,Mn)$_3$Si-type phase exhibits a transition to a ferromagnetic state at high temperature along with a low-temperature ($<$50 K) antiferromagnetic-type spin-reorientation temperature (T_R). Similar phase transitions have been observed for the compounds studied here, as indicated by the arrows in Fig. 1(c) and results presented in the Supplemental Material [15]. Without Mn, the Fe$_3$Si phase has a T_C value of around 800 K and with Mn insertion T_C rapidly decreases to values below room temperature [35,36]. A magnetic phase diagram using literature values of the (Fe,Mn)$_3$Si phase is shown in Fig. 4(d) and results of magnetic transition temperatures for the primary and secondary phases of our studied compounds as obtained from temperature-dependent magnetization measurements [cf. Fig. 1(c)] are shown in
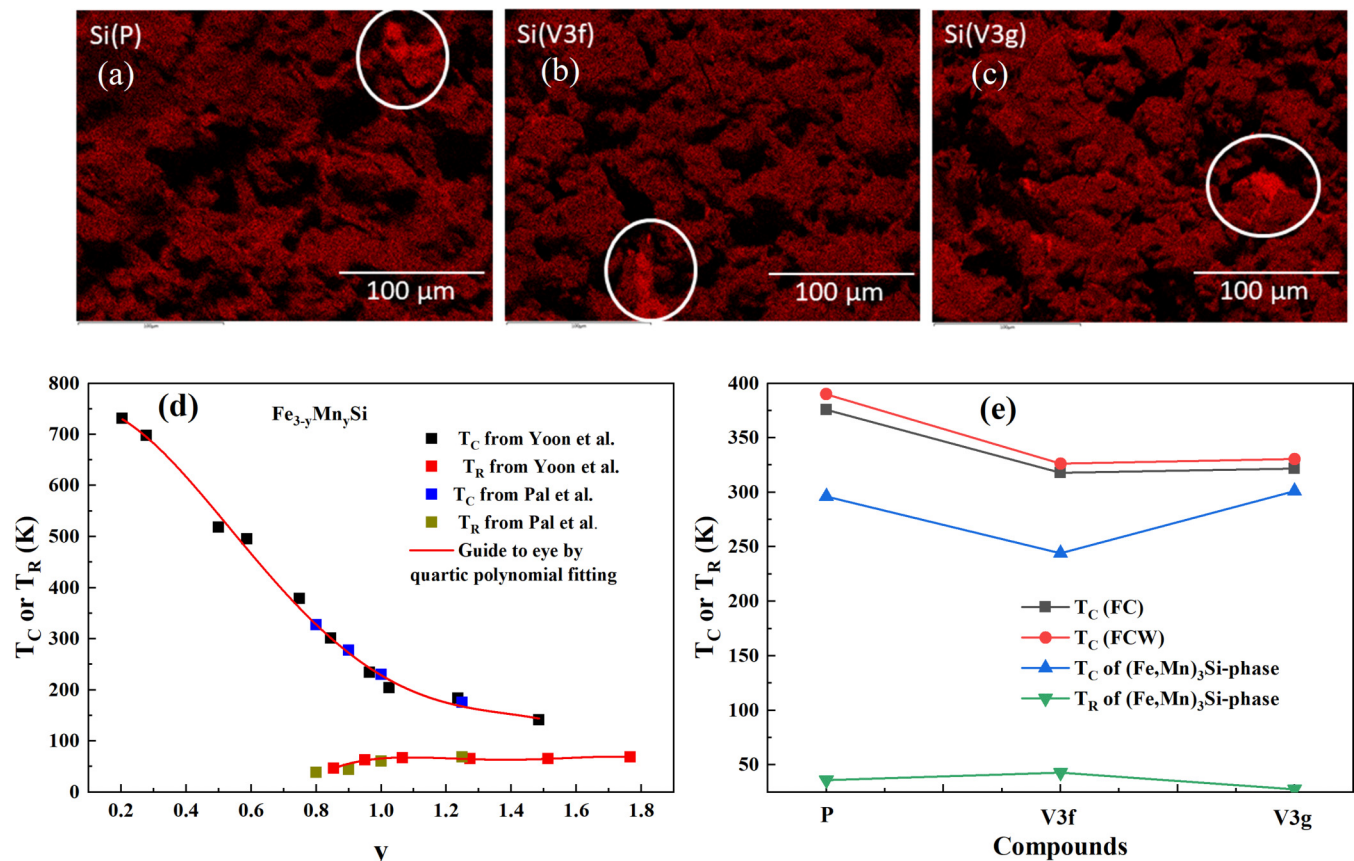

FIG. 4. (a)–(c) Elemental mapping of Si for the three studied compounds. The circled regions indicate regions with excess of Si. (d) Magnetic phase diagram of Fe$_{3-y}$Mn$_y$Si based on published literature values for the magnetic ordering temperatures. (e) T_C and T_R values for the primary and secondary phases of the studied compounds.

TABLE V. Results from formation energy calculations. The energy differences are given in units of mRy/atom.

x	ΔF_1 $(c/a = 0.53)$	ΔF_1 $(c/a = 0.58)$	ΔF_2 $(c/a = 0.53)$	ΔF_2 $(c/a = 0.58)$
0	0.000	0.000	0.000	0.000
0.01	0.947	0.681	0.949	0.969
0.02	1.797	1.328	1.849	1.391
0.03	2.630	1.946	2.735	2.079
0.04	3.367	2.546	3.511	2.759
0.05	4.182	3.126	4.347	3.373

Fig. 4(e). Comparing the measured transition temperatures of the (Fe,Mn)$_3$Si phase with the transition temperatures shown in the phase diagram, it can be concluded that the secondary phase of the V3f compound has a higher Mn to Fe ratio compared to the parent and V3g compounds. This also indicates that the V3f compound has a deficiency of Mn in the primary Fe$_2$P-type phase. Interestingly, all three compounds have been synthesized using identical conditions. Therefore the loss of Mn in the V3f compound should have some intrinsic origin.

E. Phase formation energy

To find the reason of Mn loss in the V3f compound and to estimate the effect of V substitution, the total energies of the systems have been calculated using density functional theory. For a more stable compound, the formation energy is expected to be negative and smaller relative to the pure components in their ground-state structures. For the calculation two cases have been considered.

Case 1. All Fe (Mn) atoms occupy 3f (3g) site. Therefore, the formation energy for 3f site substitution with x amount of V can be represented as,

$$\Delta F_{(Fe_{1-x}V_x)MnP_{0.5}Si_{0.5}}$$
$$= E_{(Fe_{1-x}V_x)MnP_{0.5}Si_{0.5}}$$
$$- (1-x)E_{Fe} - xE_V - E_{Mn} - 0.5E_P - 0.5E_{Si}.$$

Similarly, the formation energy for 3g site substitution will be,

$$\Delta F_{Fe(Mn_{1-x}V_x)P_{0.5}Si_{0.5}}$$
$$= E_{Fe(Mn_{1-x}V_x)P_{0.5}Si_{0.5}}$$
$$- E_{Fe} - (1-x)E_{Mn} - xE_V - 0.5E_P - 0.5E_{Si}.$$

The stoichiometries of the compounds considered for these two formation energy calculations are different, and the results establish which compound is more energetically stable. The energy difference between 3f and 3g site substitution can therefore be expressed as,

$$\Delta F_1 = E_{(Fe_{1-x}V_x)MnP_{0.5}Si_{0.5}}$$
$$- E_{Fe(Mn_{1-x}V_x)P_{0.5}Si_{0.5}} + xE_{Fe} - xE_{Mn}.$$

The value of ΔF_1 for two different c/a ratios are listed in Table V. Positive values indicate smaller formation energy for 3g site substitution. One may also note that the formation energy difference is higher for a higher level of V substitution. All these facts show that the 3g site substituted compound is
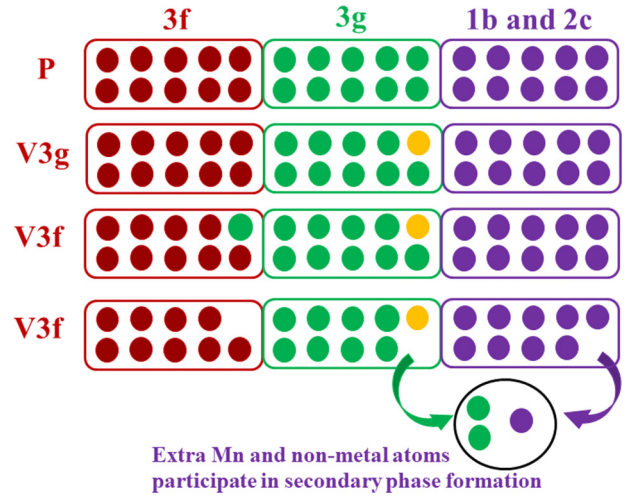

FIG. 5. Model of V (yellow circles) substitution in the Fe (red circles) and Mn (green circles) dominated 3f and 3g sites, respectively. The purple circles represent P and Si. For the V3f compound two cases with Mn occupying the 3f site and Mn leaving the Fe$_2$P phase are shown.

energetically more stable than the 3f site substituted compound.

Case 2. Although it is known from analysis of the Mössbauer results that Fe prefers to occupy the 3f site, there is no direct evidence that Mn cannot occupy the 3f site. In this particular case, the possibility of a small amount of Mn (Fe) occupying the 3f (3g) site is considered. To be more specific, the 3f site of the parent compound is fully occupied by Fe, while the 3g site is fully occupied by Mn. A small amount of V substitution (x) will be added to study if V replaces Fe (3f site) or Mn (3g site) and at the same time pushes to the other sublattice the same small amount of Fe (from 3f to 3g) or Mn (from 3g to 3f). Moreover, equimolar amounts of Fe and Mn are considered. Therefore, similar to the case 1, the formation energies for 3f and 3g site substitutions have been calculated and their difference can be expressed as (see Supplemental Material [15] for detailed calculation),

$$\Delta F_2 = E_{(Fe_{1-x}V_x)(Fe_{x/2}Mn_{1-x/2})P_{0.5}Si_{0.5}}$$
$$- E_{(Fe_{1-x/2}Mn_{x/2})(Mn_{1-x}V_x)P_{0.5}Si_{0.5}}.$$

Table V lists the values of ΔF_2 for two different c/a ratios. Similar to case 1, case 2 also indicates that the 3g site substituted compound is energetically more stable than the 3f-site-substituted compound. To understand the physical consequences of this, a simplified model (cf. Fig. 5) is considered. Ten atoms each of Fe and Mn are considered to occupy the 3f and 3g sites, respectively, as a ground state (i.e., parent compound). Now, if 1 Mn atom is replaced by 1 V atom (i.e., V3g compound), following the total energy minimum criterion, V will occupy the 3g state. As a result there will be an equimolar amount of Fe and Mn+V in the 3f and 3g sites, respectively. However, for the V3f compound, the V atom will not occupy the 3f site, it will occupy the 3g site. This can have two consequences, either one Mn atom can occupy the 3f site or an equimolar amount of metallic atoms will occupy the 3f and 3g sites and the extra Mn atom will leave the

Fe$_2$P phase and contribute to the secondary phase formation, as indicated in Fig. 5. In the first scenario, the Mn in the $3f$ site will interact antiferromagnetically with the Fe in $3f$ site [37]. In the second scenario, some amount of Mn will leave the Fe$_2$P phase of the V$3f$ compound, and participate in the secondary phase formation, which will enhance the Mn/Fe ratio of the secondary phase (Fe$_{1-x}$Mn$_x$Si). The enhancement of the Mn/Fe ratio in the V$3f$ compound has been discussed previously. Moreover, in both cases, the overall magnetization of the V$3f$ compound will decrease, which explains the observed magnetization anomaly in the saturation magnetization result.

IV. SUMMARY AND CONCLUSIONS

V substitution in the metallic sites of FeMnP$_{0.5}$Si$_{0.5}$, results in a decrease of T_C, which is proportional to the atomic distance (d_{3f-3g}) between $3f$ and $3g$ site atoms. From the Bethe-Slater curve, it is explained that the magnetic exchange interaction between $3f$ and $3g$ site atoms for the studied compounds is proportional to d_{3f-3g}. Owing to the dependence of T_C on the magnetic interaction strength, a relative change in d_{3f-3g} leads to a corresponding change in T_C. From the formation energy calculations, it was found that $3g$ site substitution is energetically favorable for the V atom. Attempting a $3f$ site substitution will provoke either antiferromagnetic interaction in the $3f$ site or a secondary phase formation with the cost of an overall decrease of the magnetization. From

Mössbauer spectroscopy of the studied compounds apart from the absence of Fe in the $3g$ site, a decrease of the hyperfine parameter *CS* (central shift) with V substitution has been observed. A larger *CS* parameter represents nonbonded or weekly bonded Fe, which is favorable for the Fe moment fluctuation across the PM-FM phase transition [30]. A larger moment fluctuation results in a larger value of $-\Delta S_M$. Therefore, a direct correlation between the *CS* parameter and the value of $-\Delta S_M$ has been evidenced. Interestingly, the value of the temperature hysteresis ΔT_{hys} decreases with V substitution. The ΔT_{hys} in the Fe$_2$P-type systems originates from the energy barrier between the states characterized by different *c* and *a* lattice parameters (described by $\Delta a/a$ and $\Delta c/c$). Here, in this work we have shown that with V substitution the energy barrier decreases considerably and results in a decrease of ΔT_{hys}, which is highly desirable for the magnetic refrigeration application.

ACKNOWLEDGMENTS

[1] K. Gschneidner Jr and V. Pecharsky, Thirty years of near room temperature magnetic cooling: Where we are today and future prospects, Int. J. Refrig. **31**, 945 (2008).

[2] J. Lyubina, Magnetocaloric materials for energy efficient cooling, J. Phys. D **50**, 053002 (2017).

[3] O. Gutfleisch, T. Gottschall, M. Fries, D. Benke, I. Radulov, K. P. Skokov, H. Wende, M. Gruner, M. Acet, P. Entel *et al.*, Mastering hysteresis in magnetocaloric materials, Philos. Trans. R. Soc. A **374**, 20150308 (2016).

[4] L. F. Cohen, Contributions to hysteresis in magnetocaloric materials, physica status solidi (b) **255**, 1700317 (2018).

[5] X. F. Miao, L. Caron, P. Roy, N. H. Dung, L. Zhang, W. A. Kockelmann, R. A. De Groot, N. Van Dijk, and E. Brück, Tuning the phase transition in transition-metal-based magnetocaloric compounds, Phys. Rev. B **89**, 174429 (2014).

[6] X. F. Miao, L. Caron, J. Cedervall, P. C. M. Gubbens, P. Dalmas de Réotier, A. Yaouanc, F. Qian, A. R. Wildes, H. Luetkens, A. Amato, N. H. van Dijk, and E. Brück, Short-range magnetic correlations and spin dynamics in the paramagnetic regime of (Mn, Fe)$_2$ (P, Si), Phys. Rev. B **94**, 014426 (2016).

[7] N. H. Dung, Z. Q. Ou, L. Caron, L. Zhang, D. T. C. Thanh, G. A. De Wijs, R. A. De Groot, K. J. Buschow, and E. Brück, Adv. Energy Mater. **1**, 1215 (2011).

[8] J. Lai, B. Huang, X. Miao, N. Van Thang, X. You, M. Maschek, L. van Eijck, D. Zeng, N. van Dijk, and E. Brück, Combined effect of annealing temperature and vanadium substitution for mangetocaloric Mn$_{1.2-x}$V$_x$Fe$_{0.75}$P$_{0.5}$Si$_{0.5}$ alloys, J. Alloys Compd. **803**, 671 (2019).

[9] J. Lai, X. You, I. Dugulan, B. Huang, J. Liu, M. Maschek, L. van Eijck, N. van Dijk, and E. Brück, Tuning the magnetoelastic transition of (Mn,Fe,V)$_2$(P,Si) alloys to low magnetic field applications, J. Alloys Compd. **821**, 153451 (2020).

[10] M. Hudl, L. Häggström, E.-K. Delczeg-Czirjak, V. Höglin, M. Sahlberg, L. Vitos, O. Eriksson, P. Nordblad, and Y. Andersson, Strongly enhanced magnetic moments in ferromagnetic FeMnP$_{0.5}$Si$_{0.5}$, Appl. Phys. Lett. **99**, 152502 (2011).

[11] B. Carlsson, M. Gölin, and S. Rundqvist, Determination of the homogeneity range and refinement of the crystal structure of Fe$_2$P, J. Solid State Chem. **8**, 57 (1973).

[12] A. A. Coelho, TOPAS and TOPAS-Academic: An optimization program integrating computer algebra and crystallographic objects written in C++, J. Appl. Crystallogr **51**, 210 (2018).

[13] L. Vitos, *Computational Quantum Mechanics for Materials Engineers: The EMTO Method and Applications* (Springer Science & Business Media, Berlin, 2007).

[14] J. P. Perdew, K. Burke, and M. Ernzerhof, Generalized Gradient Approximation Made Simple, Phys. Rev. Lett. **77**, 3865 (1996).

[15] See Supplemental Material at http://link.aps.org/supplemental/10.1103/PhysRevB.107.104409 for a detailed description of the effect of secondary phase, lattice parameter calculations, and formation energy calculations.

[16] K. A. Gschneidner, V. Pecharsky, and A. Tsokol, Recent developments in magnetocaloric materials, Rep. Prog. Phys. **68**, 1479 (2005).

[17] L. Caron, Z. Ou, T. Nguyen, D. C. Thanh, O. Tegus, and E. Brück, On the determination of the magnetic entropy change

in materials with first-order transitions, J. Magn. Magn. Mater. **321**, 3559 (2009).

[18] K. Gschneidner Jr and V. K. Pecharsky, Magnetocaloric materials, Annu. Rev. Mater. Res. **30**, 387 (2000).

[19] B. Shen, J. Sun, F. Hu, H. Zhang, and Z. Cheng, Recent progress in exploring magnetocaloric materials, Adv. Mater. **21**, 4545 (2009).

[20] M.-H. Phan and S.-C. Yu, Review of the magnetocaloric effect in manganite materials, J. Magn. Magn. Mater. **308**, 325 (2007).

[21] R. Skini, S. Ghorai, P. Ström, S. Ivanov, D. Primetzhofer, and P. Svedlindh, Large room temperature relative cooling power in $La_{0.5}Pr_{0.2}Ca_{0.1}Sr_{0.2}MnO_3$, J. Alloys Compd. **827**, 154292 (2020).

[22] C.-B. Rong and J. P. Liu, Temperature- and magnetic-field-induced phase transitions in Fe-rich FePt alloys, Appl. Phys. Lett. **90**, 222504 (2007).

[23] N. Trung, Z. Ou, T. Gortenmulder, O. Tegus, K. Buschow, and E. Brück, Tunable thermal hysteresis in MnFe (P, Ge) compounds, Appl. Phys. Lett. **94**, 102513 (2009).

[24] D. Cam Thanh, E. Brück, N. Trung, J. Klaasse, K. Buschow, Z. Ou, O. Tegus, and L. Caron, Structure, magnetism, and magnetocaloric properties of Mn Fe P_{1-x} Six compounds, J. Appl. Phys. **103**, 07B318 (2008).

[25] S. Ghorai, R. Skini, D. Hedlund, P. Ström, and P. Svedlindh, Field induced crossover in critical behaviour and direct measurement of the magnetocaloric properties of $La_{0.4}Pr_{0.3}Ca_{0.1}Sr_{0.2}MnO_3$, Sci. Rep. **10**, 19485 (2020).

[26] X. F. Miao, Y. Mitsui, A. I. Dugulan, L. Caron, N. V. Thang, P. Manuel, K. Koyama, K. Takahashi, N. H. Van Dijk, and E. Brück, Kinetic-arrest-induced phase coexistence and metastability in (Mn, Fe)$_2$ (P, Si), Phys. Rev. B **94**, 094426 (2016).

[27] J. Cedervall, M. S. Andersson, E. K. Delczeg-Czirjak, D. Iuşan, M. Pereiro, P. Roy, T. Ericsson, L. Häggström, W. Lohstroh, H. Mutka, M. Sahlberg, P. Nordblad, and P. P. Deen, Magnetocaloric effect in Fe$_2$P: Magnetic and phonon degrees of freedom, Phys. Rev. B **99**, 174437 (2019).

[28] K. Azumi and J. Goldman, Volume magnetostriction in nickel and the bethe-slater interaction curve, Phys. Rev. **93**, 630 (1954).

[29] M. Boeije, P. Roy, F. Guillou, H. Yibole, X. Miao, L. Caron, D. Banerjee, N. Van Dijk, R. De Groot, and E. Brück, Efficient room-temperature cooling with magnets, Chem. Mater. **28**, 4901 (2016).

[30] X.-F. Miao, S.-Y. Hu, F. Xu, and E. Brück, Overview of magnetoelastic coupling in (Mn, Fe)$_2$ (P, Si)-type magnetocaloric materials, Rare Metals **37**, 723 (2018).

[31] N. H. Dung, L. Zhang, Z. Q. Ou, and E. Brück, Magnetoelastic coupling and magnetocaloric effect in hexagonal Mn–Fe–P–Si compounds, Scr. Mater. **67**, 975 (2012).

[32] D. Fruchart, S. Haj-Khlifa, P. de Rango, M. Balli, R. Zach, W. Chajec, P. Fornal, J. Stanek, S. Kaprzyk, and J. Tobola, Structure and magnetic properties of bulk synthesized $Mn_{2-x}Fe_xP_{1-y}Si_y$ compounds from magnetization, ^{57}Fe Mössbauer spectroscopy, and electronic structure calculations, Crystals **9**, 37 (2019).

[33] H. Tian, W. Zheng, B. Zheng, X. Wang, Q. Wen, T. Ding, and Z. Zhao, Dynamic isomer shift in charge-ordering manganite $Y_{0.5}Ca_{0.5}MnO_3$: Mössbauer spectroscopy study, J. Phys. Chem. B **109**, 1656 (2005).

[34] K. N. Shrivastava, Reexamination of the Mössbauer isomer shift, Phys. Rev. B **1**, 955 (1970).

[35] S. Yoon and J. Booth, Structural and magnetic properties of $Fe_{3-x}Mn_xSi$ alloys, Phys. Lett. A **48**, 381 (1974).

[36] L. Pal, K. Suresh, and A. Nigam, Effect of mn substitution on the magnetic and magneto-transport properties of $Fe_{3-x}Mn_xSi$ ($0 \leqslant x \leqslant 1.25$) alloys, J. Appl. Phys. **113**, 093904 (2013).

[37] E. K. Delczeg-Czirjak, M. Pereiro, L. Bergqvist, Y. O. Kvashnin, I. Di Marco, G. Li, L. Vitos, and O. Eriksson, Origin of the magnetostructural coupling in $FeMnP_{0.75}Si_{0.25}$, Phys. Rev. B **90**, 214436 (2014).